

Interaction of a soliton with a localized gain in a fiber Bragg grating

William C. K. Mak¹, Boris A. Malomed^{2,1}, and Pak L. Chu¹

¹*Optoelectronic Research Centre, Department of Electronic Engineering, City University of Hong Kong, Tat Chee Avenue, Kowloon, Hong Kong and*

²*Department of Interdisciplinary Studies, Faculty of Engineering, Tel Aviv University, Tel Aviv 69978, Israel*

Abstract

A model of a lossy nonlinear fiber grating with a “hot spot”, which combines a local gain and an attractive perturbation of the refractive index, is introduced. A family of exact solutions for pinned solitons is found in the absence of loss and gain. In the presence of the loss and localized gain, an instability threshold of the zero solution is found. If the loss and gain are small, it is predicted what soliton is selected by the energy-balance condition. Direct simulations demonstrate that only one pinned soliton is stable in the conservative model, and it is a *semi – attractor*: solitons with a larger energy relax to it via emission of radiation, while those with a smaller energy decay. The same is found for solitons trapped by a pair of repulsive inhomogeneities. In the model with the loss and gain, stable pinned pulses demonstrate persistent internal vibrations and emission of radiation. If these solitons are nearly stationary, the prediction based on the energy balance underestimates the necessary gain by 10 – 15% (due to radiation loss). If the loss and gain are larger, the intrinsic vibrations of the pinned soliton become chaotic. The local gain alone, without the attractive perturbation of the local refractive index, cannot maintain a stable pinned soliton. For collisions of moving solitons with the “hot spot”, passage and capture regimes are identified, the capture actually implying splitting of the soliton.

PACS numbers:

I. INTRODUCTION

Solitons in any physical medium are subject to attenuation due to dissipation, hence it is necessary to apply gain which can support the solitons. A possibility which may find interesting physical applications is to create a localized gain, which will be a trap for solitons in a lossy medium. In terms of optical solitons, this can be easily realized for spatial solitons in a planar waveguide, where the gain may be applied to a narrow strip. However, for spatial solitons gain is a redundancy, as they are supported simply by the energy flux through the soliton itself. Besides that, in this work it will be shown that, in the simplest case when the spatial solitons are governed by the nonlinear Schrödinger (NLS) equation, a pinned soliton supported by the localized gain can never be stable. On the other hand, realization of the local-gain trap for usual temporal solitons is impossible, as such a soliton runs (for instance, in an optical fiber [1]) with the group velocity of light.

An unique possibility to create a gain-induced trap in a lossy medium is offered by a fiber grating, i.e., a Bragg grating (BG) written on an optical fiber. Fiber gratings are a basis for many photonic devices [2]. A challenging possibility is to use fiber gratings for the creation of pulses of slow light, which is a topic of great current interest [3]. The possibility of the existence of slow pulses suggest to try a local-gain-induced trap for solitons.

In fiber gratings, solitons exist due to the interplay between the Bragg reflection and Kerr nonlinearity of the BG-carrying fiber [4]. These solitons were predicted analytically [5, 6], and then they were created in the experiment [7]. Except for the case in which the BG soliton is very broad [8], this species of optical solitons is distinct from the usual nonlinear-Schrödinger (NLS) solitons [1] in ordinary nonlinear optical fibers.

As it was mentioned above, search for very slow solitons in fiber gratings, which were predicted long ago [6], is an issue of great interest [9]. The standard mathematical model of the nonlinear fiber grating predicts a whole family of zero-velocity solitons [4, 5, 6], a part of which is stable [10, 11]. If realized experimentally, such a soliton would represent a pulse of standing light, with its left- and right-traveling components being in a permanent dynamical equilibrium.

The BG solitons which have been observed in the experiment up to date are moving ones, their velocity being $\simeq 75\%$ of the maximum group velocity of light in the fiber [7]. The quest for zero-velocity solitons may be facilitated by means of a local defect in the BG that exerts

an attractive force on a soliton, having thus a potential to be a soliton trap (note that a local defect may trap light in the fiber grating via the four-wave mixing without formation of a soliton [12]). Besides its profound physical importance [13], such a soliton trap is also promising for the fiber-sensing technology [14].

The interaction of the soliton with an attractive defect in the form of a local suppression of BG was studied recently in Refs. [13] and [14]. The latter work also considered a trap combining the local BG suppression and a change in the refractive index (these two effects may come together as a manifestation of a local inhomogeneity in the BG-carrying fiber). As a result, it has been demonstrated that a gap soliton may indeed be pinned by the local defect, and, moreover, a narrow (delta-functional) defect uniquely selects parameters of the stable trapped soliton [14] (this feature is described in more detail below).

However, a trapped soliton will be destroyed by fiber loss. Indeed, taking into regard that the best fiber gratings (used as dispersion compensators in optical telecommunications [15]) have the attenuation rate $\simeq 0.2$ dB/cm (in hybrid grating waveguides, using glass and a sol-gel material, the attenuation may be lowered to 0.1 dB/cm [16]), it is easy to estimate that a standing soliton will be destroyed during the time $\lesssim 5$ ns. Therefore, it is necessary to support the trapped soliton by means of a locally applied optical gain, which is tantamount to the above-mentioned soliton trap induced by local gain. A related problem is a possibility to capture a moving soliton by the local gain. These issues are the main subjects of the present work. Besides the fundamental interest to having permanently maintained trapped optical solitons, they may also be interesting for applications, such as optical memory.

The local gain can be provided, for instance, by a short resonantly doped segment in the BG-carrying fiber. In this connection, we note that the moving BG soliton that was observed for the first time in the fiber grating had the temporal width $\simeq 200$ ps [7]. Taking into regard the Lorentzian contraction (as it was mentioned above, the soliton was moving at a velocity equal $\approx 75\%$ of the maximum group velocity), the same soliton, if stopped, would have the spatial width on the order of a few centimeters. Thus, the locally pumped segment of the fiber may be approximated by a delta-function (which we assume in the analytical model below) if, roughly speaking, its size is $\simeq 1$ mm. Note that the maximum gain that can be provided by an Er-doped amplifier is $\simeq 5$ dB/cm [17]. Comparing this to the above-mentioned minimum damping rate 0.1 dB/cm, we conclude that the proposed scheme may be self-consistent.

Thus, the model to be formulated below assumes the local gain in the form of the delta-function (in the numerical part of the work, a smooth approximation to the delta-function is used). The model also includes an imaginary part of the localized gain, which actually accounts for a local perturbation of the fiber’s refractive index (note that the dopant, if used to induce the local gain, may indeed affect the local refractive index). The imaginary part is necessary, as it will be seen that pure gain cannot maintain a pinned soliton in a stable state. As for the size of the refractive-index perturbation δn , it will be seen that $\delta n \gtrsim 0.1$ is definitely sufficient to stably trap a soliton. In this respect, it is relevant to mention that a dopant added to a silica fiber usually induces a refractive index change $\delta n \sim 0.05$, while in a polymer fiber it is ~ 0.2 . The latter value can readily produce a stable pinned state of the soliton, and the former one may be sufficient too.

A relatively large jump of the refractive index between the doped segment and the rest of the fiber may induce an additional effect, viz., reflection of light, although the reflection may be smothered by a sufficiently smooth profile of distribution of the dopant. An additional term in the basic model [see Eqs. (1) and (2) below], induced by the reflection, would be the same which formally accounts for a local perturbation of the BG reflectivity. The latter type of the conservative perturbation was considered in Ref. [14]), a conclusion being that its effect is quite similar to that directly produced by the refractive-index perturbation, which is directly included in Eqs. (1) and (2). For this reason, we do not consider the local reflection as a separate perturbation in this work (in any case, it can be easily added, if necessary).

The paper is organized as follows. In section 2 we formulate the model, and produce some analytical results. First of all, we consider the stability of the zero solution against small perturbations in the presence of the uniform loss and localized loss. An instability-onset threshold is found, and it is demonstrated that the instability does not take place unless the gain has an imaginary part. For the comparison’s sake, we also briefly consider an allied model problem, viz., the instability induced by a “hot spot” in the lossy NLS equation, which produces quite similar results. Then, we produce a family of exact analytical solutions for solitons pinned by the local inhomogeneity of the refractive index, in the absence of loss and gain. Another analytical result predicts what particular pinned soliton is selected by the balance of the loss and gain, provided that they are small perturbations. A soliton selected by the energy balance is also found in the lossy NLS equation with the hot spot (in that case, it is always unstable).

Section 3 reports results of direct simulations of pinned solitons, in both the conservative version of the model, and in the full one. A surprising result is that, in the conservative model, a *single* pinned soliton, out of their continuous family, is stable. If the initially created soliton has larger energy, it relaxes, via emission of radiation, to the stable one, and if the energy of the initial soliton is smaller than that of the stable one, the pulse decays into radiation; the former observation can be explained by known results for the stability of the ordinary solitons in the unperturbed BG model [10, 11]. A similar result is also obtained, in the framework of the conservative model, at the end of section 3 for a pair of repulsive defects: in the case when they can hold a soliton at the midpoint between them, any pulse either relaxes to a uniquely selected soliton, or decays (if the pair of repulsive inhomogeneities cannot hold a soliton, it splits the soliton in two). It is relevant to mention that a nonlinear BG structure with two local defects was very recently studied as a promising model for all-optical switching [18].

In the full model, all the pinned solitons demonstrate persistent intrinsic vibrations; depending on the ratio of the loss and gain, and on the strength of the attractive refractive-index inhomogeneity, the amplitude of the vibrations may be small or large. In the former case, the pinned soliton may be regarded as an approximately stationary one, then the above-mentioned analytical prediction of the soliton selected by the balance between the loss and gain gives an error between 10% and 15%, which may be explained by extra radiation loss.

In section 4, collision of a moving soliton with the hot spot is considered by means of direct simulations. As a result, regions of passage and capture are identified in the soliton's parameter space in both the conservative and full models. In fact, the capture is incomplete: a part of the soliton's energy gets trapped, giving rise to a pinned soliton, while the other part passes and rearranges itself into another soliton. If the inhomogeneity is strong, a conspicuous part of the energy may bounce back.

II. THE MODEL AND ANALYTICAL RESULTS

A. The model equations

A localized gain inserted into a fiber grating is modelled by a δ - function term added to the standard BG model, which includes coupled equations for the amplitudes of the right-

and left-travelling electromagnetic waves, $u(x, t)$ and $v(x, t)$ [4]. The full model is then

$$iu_t + iu_x + v + (|u|^2 + 2|v|^2)u = -i\gamma u + i\Gamma\delta(x) \cdot u, \quad (1)$$

$$iv_t - iv_x + u + (|v|^2 + 2|u|^2)v = -i\gamma v + i\Gamma\delta(x) \cdot v, \quad (2)$$

where the maximum group velocity of light is normalized to be 1, the nonlinear terms account for the self- and cross-phase modulation induced by the Kerr effect, the linear couplings represent the mutual conversion of the waves due to the resonant Bragg scattering (the conversion coefficient is also normalized to be 1). On the right-hand side of Eqs. (1) and (2), the fiber loss parameter γ is real and positive, while the local-gain strength Γ may be complex,

$$\Gamma \equiv \Gamma_1 + i\Gamma_2, \quad (3)$$

its positive real part being the gain proper, while the imaginary part accounts for a localized perturbation of the refractive index (note that $\Gamma_2 > 0$ corresponds to a local increase of the refractive index).

A stationary solution, which represents a soliton trapped by the “hot spot”, is sought for as

$$u(x, t) = U(x) \exp(-it \cos \theta), \quad v(x, t) = V(x) \exp(-it \cos \theta), \quad (4)$$

where θ is a parameter of the soliton family. The substitution of Eqs. (4) into Eqs. (1) and (2) leads to equations

$$\left[i \frac{d}{dx} + \cos \theta + i\gamma + i\Gamma\delta(x) + (|U|^2 + 2|V|^2) \right] U + V = 0, \quad (5)$$

$$\left[-i \frac{d}{dx} + \cos \theta + i\gamma + i\Gamma\delta(x) + (|V|^2 + 2|U|^2) \right] V + U = 0. \quad (6)$$

B. Stability of the zero solution

We start the analysis with the linearized version of Eqs. (1) and (2), in order to analyze the stability of the zero solution in the presence of the localized gain. An eigenmode of small perturbations is sought for as

$$u(x, t) = A_+ \exp(-i\chi t - \kappa x), \quad v(x, t) = B_+ \exp(-i\chi t - \kappa x) \quad \text{at } x > 0, \quad (7)$$

$$u(x, t) = A_- \exp(-i\chi t + \kappa x), \quad v(x, t) = B_- \exp(-i\chi t + \kappa x) \quad \text{at } x < 0, \quad (8)$$

where the frequency χ may be complex, its imaginary part being the instability growth rate, and κ must have a positive real part. Substituting this into the linearized equations yields

$$\kappa = \sqrt{1 - (\chi + i\gamma)^2}, \quad (9)$$

where the square root is defined so that its real part is positive, and $B_{\pm} = -[(\chi + i\gamma) \mp i\kappa] A_{\pm}$. Further, the integration of the linearized equations in an infinitesimal vicinity of $x = 0$ yields $A_+ = A_- e^{\Gamma}$, $B_+ = B_- e^{-\Gamma}$.

Eliminating the amplitudes A_{\pm} and B_{\pm} by means of these relations, we obtain an equation

$$\frac{\chi + i\gamma - i\kappa}{\chi + i\gamma + i\kappa} = e^{-2(\Gamma_1 + i\Gamma_2)}, \quad (10)$$

where the expression (3) was substituted for Γ . Finally, combining Eqs. (10) and (9), we can find the eigenfrequency sought for:

$$\chi = -i\gamma + \text{sgn}(\sin \Gamma_2) \cdot \cosh(\Gamma_1 + i\Gamma_2), \quad (11)$$

where the sign multiplier in front of the second term provides for the fulfillment of the above-mentioned condition $\text{Re } \kappa > 0$.

A straightforward consequence of Eq. (11) is an expression for the instability growth rate,

$$\text{Im } \chi = -\gamma + (\sinh \Gamma_1) |\sin \Gamma_2|. \quad (12)$$

Thus, the localized gain gives rise to the instability of the trivial solution, provided that it is strong enough:

$$\sinh \Gamma_1 > \sinh((\Gamma_1)_{\text{cr}}) \equiv \frac{\gamma}{|\sin \Gamma_2|}. \quad (13)$$

Note that the instability is *impossible* in the absence of the local refractive-index perturbation Γ_2 . The instability-onset condition (13) simplifies in the limiting case when both the loss and gain parameters are small (while Γ_2 is not necessarily small):

$$\Gamma_1 > (\Gamma_1)_{\text{cr}} \approx \frac{\gamma}{|\sin \Gamma_2|}. \quad (14)$$

Lastly, we notice that the instability is oscillatory: as it follows from Eq. (11), $\text{Re } \chi \neq 0$, unless $\cos \Gamma_2 = 0$.

As the onset of instability in a system combining uniform loss and local gain is a simple but new issue, for the comparison's sake it is relevant to briefly consider it in a similar model, viz., the NLS equation:

$$iu_t + \frac{1}{2}Du_{xx} + |u|^2u = -i\gamma u + (i\Gamma_1 - \Gamma_2)\delta(x) \cdot u, \quad (15)$$

where D is the spatial-dispersion coefficient, γ and $\Gamma_{1,2}$ having the same meaning as above. If the variable t in Eq. (15) is replaced by the propagation distance z , and x is realized as the transverse coordinate in a planar lossy waveguide, Eq. (15) may be interpreted as describing spatial solitons in the above-mentioned case when the gain is applied along a narrow strip in the waveguide. In fact, the NLS model is a limit case of the BG system for small-amplitude solitons (see, e.g., Ref. [8]); accordingly, Eq. (15) is a small-amplitude limit of Eqs. (1) and (2). Nevertheless, it is pertinent to consider the NLS model parallel to the BG one, as it will help to understand the results for the BG system.

A perturbation mode in the linearized equation (15) is sought for as [cf. Eqs. (7) and (8)]

$$u(x, t) = A_+ \exp(-i\chi t - \kappa x) \text{ at } x > 0, \quad u(x, t) = A_- \exp(-i\chi t + \kappa x) \text{ at } x < 0, \quad (16)$$

with $\text{Re } \kappa > 0$. The substitution of Eq. (16) into the linearized version of Eq. (15) yields

$$\chi = - \left[(D/2) \kappa^2 + i\gamma \right], \quad (17)$$

and the integration of Eq. (15) in an infinitesimal vicinity of $x = 0$ leads to $A_+ = A_-$, and

$$D\kappa = \Gamma_2 - i\Gamma_1. \quad (18)$$

Note that the necessary condition $\text{Re } \kappa > 0$ and Eq. (18) show that, in fact, the perturbation mode (16) exists only in the case $\Gamma_2 D > 0$. It is easy to understand the meaning of the latter condition: the inhomogeneity is *attractive* in this case, hence it can support the local mode.

The substitution of Eq. (18) into Eq. (17) yields a final result,

$$\chi = - \left[\frac{(\Gamma_2 - i\Gamma_1)^2}{2D} + i\gamma \right]. \quad (19)$$

As it follows from Eq. (19), the instability-onset condition, $\text{Im } \chi > 0$, means, in the present case,

$$\Gamma_1 > (\Gamma_1)_{\text{cr}} \equiv D\gamma/\Gamma_2. \quad (20)$$

Thus, as well as in the case of the hot spot in BG, Eq. (20) demonstrates that the hot spot in the NLS model cannot give rise to the instability, unless it contains the imaginary part. Unlike the BG model, the additional condition $\Gamma_2 D > 0$ is also necessary for the instability.

C. An exact solution in the conservative model

An exact solution for the pinned soliton is available for the conservative version of the full nonlinear model, with $\gamma = \Gamma_1 = 0$. In this case, it is easy to see that Eqs. (5) and (6) admit an invariant reduction, $V(x) = -U^*(x)$ (the asterisk stands for the complex conjugation), which leads to a single equation,

$$\left[i \frac{d}{dx} U + \Gamma_2 \cos \theta + \delta(x) \right] U + 3|U|^2 U - U^* = 0. \quad (21)$$

As it follows from the integration of Eq. (21) around the point $x = 0$, the solution must satisfy a boundary condition

$$U(x = +0) = U(x = -0) \cdot \exp(i\Gamma_2). \quad (22)$$

An exact soliton-like solution to Eq. (21), supplemented by the condition (22), can be found, following the pattern of the exact solution for the ordinary gap soliton in the model with $\Gamma_2 = 0$ [5]:

$$U(x) = \frac{1}{\sqrt{3}} \frac{\sin \theta}{\cosh \left[(x + a \operatorname{sgn} x) \sin \theta - \frac{i}{2} \theta \right]}, \quad (23)$$

where $\operatorname{sgn} x \equiv \pm 1$ for positive and negative x , and the real parameter a is determined by the relation

$$\tanh(a \sin \theta) = \frac{\tan(\Gamma_2/2)}{\tan(\theta/2)}. \quad (24)$$

A corollary of the expressions (23) and (24), that will be used below, is

$$|U(x=0)|^2 = \frac{2}{3} (\cos \Gamma_2 - \cos \theta). \quad (25)$$

From Eq. (24) it follows that the solution exists not in the whole interval $0 < \theta < \pi$, where the ordinary gap solitons are found, but in a region determined by the constraint that $|\tanh(a \sin \theta)| < 1$, i.e., $|\tan(\Gamma_2/2)| < \tan(\theta/2)$, or

$$|\Gamma_2| < \theta < \pi \quad (26)$$

(which implies that the solutions exist only if $|\Gamma_2| < \pi$).

Although the exact solutions found above exist for either sign of Γ_2 , it is expected that only in the case $\Gamma_2 > 0$ they may be stable, as in this case the local inhomogeneity *attracts* the soliton (which is natural, as positive Γ_2 corresponds to a local enhancement of the

refractive index, and a bright soliton is always attracted to an optically denser spot) [14]. In particular, in the case of small Γ_2 the soliton may be regarded as a quasiparticle in an effective inhomogeneity-induced potential

$$W_1(\xi) = -\frac{8\Gamma_2}{3} \frac{\sin^2 \theta}{\cosh(2\xi \sin \theta) + \cos \theta}, \quad (27)$$

where ξ is a displacement of the soliton's center from the point $x = 0$ [14]. It is obvious that this potential indeed corresponds to the attraction and repulsion in the cases $\Gamma_2 > 0$ and $\Gamma_2 < 0$.

Note that the exact solution is a single-humped one, with a maximum at the point $x = 0$, if $\Gamma_2 > 0$; in the opposite case, the solution is a double-humped, with a local minimum at $x = 0$ and local maxima at $x = \pm |a|$, as in this case Eq. (24) gives $a < 0$. In the limiting case $\theta - |\Gamma_2| \rightarrow 0$ [see Eq. (26)], Eq. (25) shows that $|U(x = 0)|$ vanishes, i.e., the soliton pinned by the attractive inhomogeneity, with $\Gamma_2 > 0$, reduces to zero, while the unstable two-humped state pinned by the repulsive inhomogeneity, with $\Gamma_2 < 0$, goes over into a pair of two infinitely separated solitons with $\theta = -\Gamma_2$.

D. The first-order approximation for the full model

In the case $\gamma = \Gamma_1 = 0$, Eqs. (1) and (2) conserve the net energy,

$$E = \int_{-\infty}^{+\infty} [|u(x)|^2 + |v(x)|^2] dx. \quad (28)$$

In the presence of the loss and gain, the exact evolution equation for the energy is

$$\frac{dE}{dt} = -2\gamma E + 2\Gamma_1 [|u(x)|^2 + |v(x)|^2] |_{x=0}. \quad (29)$$

If the coefficients γ and Γ_1 are treated as small perturbations, the balance condition for the energy, $dE/dt = 0$, may select a particular solution, from the family of the exact solutions (23) of the conservative model, which remains, to the first approximation, a stationary pinned soliton in the full model.

The balance condition following from Eq. (29) demands

$$\gamma E = \Gamma_1 [|U(x = 0)|^2 + |V(x = 0)|^2]. \quad (30)$$

Substituting, in the first approximation, the unperturbed solution (23) and (24) into Eq. (30), and taking into regard the definition (28), the balance condition can be cast, after

some algebra, in a simple form:

$$\frac{\theta - \Gamma_2}{\cos \Gamma_2 - \cos \theta} = \frac{\Gamma_1}{\gamma}. \quad (31)$$

As the pinned soliton may only be stable if $\Gamma_2 > 0$, we consider this case. Note also that, according to Eq. (26), we should constrain the consideration to the interval $\theta > \Gamma_2$, as otherwise the pinned solitons do not exist in the zero approximation ($\gamma = \Gamma_1 = 0$).

The pinned soliton selected by Eq. (31) is expected to appear, with the increase of the *stress parameter* Γ_1/γ , as a result of some bifurcation. The inspection of Fig. 1, which displays $(\theta - \Gamma_2)$ vs. Γ_1/γ , as found from Eq. (31), shows that the situation is qualitatively different in the cases $\Gamma_2 < \pi/2$ and $\Gamma_2 > \pi/2$.

In the former case, a *tangent* (saddle-node) bifurcation [19] occurs at a minimum value $(\Gamma_1/\gamma)_{\min}$ of the stress parameter at which Eq. (31) has a physical solution for θ , and two solutions exist for $\Gamma_1/\gamma > (\Gamma_1/\gamma)_{\min}$. An additional analysis of Eq. (31) demonstrates that, with the variation of Γ_2 , the value $(\Gamma_1/\gamma)_{\min}$ attains an absolute minimum, $\Gamma_1/\gamma = 1$, at $\Gamma_2 = \pi/2$.

With the increase of Γ_1/γ , the lower solution branch that starts at the saddle-node bifurcation point [see Fig. 1(a)] hits the limit point $\theta = \Gamma_2$ [see Eq. (26)], where it degenerates into the zero solution, according to Eq. (25). Equation (31) shows that this happens at the point $\Gamma_1/\gamma = 1/\sin \Gamma_2$. On the other hand, it was shown above [see Eq. (14)] that, precisely at the same point, the zero solution becomes unstable, in the limit of small Γ_1 and γ . According to the general stability-exchange principle [19], the fact that the zero-solution branch gets unstable after its collision with another solution branch implies that the latter branch was already unstable. Therefore, we conclude that the branch which appears at the saddle-node bifurcation and ceases to exist hitting the zero solution, is an unstable saddle.

The other (upper) branch generated by the saddle-node bifurcation [Fig. 1(a)] continues until it attains the maximum value $\theta = \pi$ relevant to the physical solutions, which happens at

$$\frac{\Gamma_1}{\gamma} = \left(\frac{\Gamma_1}{\gamma} \right)_{\max} \equiv \frac{\pi - \Gamma_2}{1 + \cos \Gamma_2}. \quad (32)$$

This branch corresponds to the node-type solution which appears at the saddle-node bifurcation point, therefore it has a chance to be stable. However, it may be unstable against perturbations that are not taken into regard by this elementary consideration (for instance, the possibility of a shift of the soliton's center from the point $x = 0$ was not taken into

regard). The actual situation with the stability of pinned solitons in the model including the loss and gain is rather complicated, see the next section.

In the case $\Gamma_2 > \pi/2$, the situation is different, as the saddle-node bifurcation is imaginary in this case, occurring in the unphysical region $\theta < \Gamma_2$, see Fig. 1(b). The only physical branch of the solutions appears at the point $\Gamma_1/\gamma = 1/\sin \Gamma_2$, where it crosses the zero solution, lending it the instability, which the branch presumably had in the unphysical region. The stability-exchange principle which was already mentioned above suggests that, from the viewpoint of the present analysis, this branch becomes stable when it crosses into the physical region, $\theta > \Gamma_2$. However, as well as the other branch considered above for the case $\Gamma_2 < \pi/2$, the present one may be subject to instabilities of other types. This branch ceases to be a physical one at the point (32).

At the border between the two generic cases considered above, i.e., at $\Gamma_2 = \pi/2$, the saddle-node bifurcation occurs exactly at the point $\theta = \pi/2$, see Fig. 1(c). In this case, the destabilization of the zero solution happens at the same point.

The situation is different in the case $\Gamma_2 = 0$ [see Fig. 1(d)], when the hot spot has no refractive-index-perturbation component, and Eq. (31) takes the form

$$\frac{\theta}{2 \sin^2(\theta/2)} = \frac{\Gamma_1}{\gamma}. \quad (33)$$

In this case, as it was stressed above, the zero solution is never destabilized, in accordance with which the solution branches do not cross the axis $\theta = 0$ in Fig. 1(d). The lower branch, which asymptotically approaches the $\theta = 0$ axis, must be unstable (this is a generic feature in the case when the amplitude of the solution decreases with the increase of the stress parameter [19]), hence the upper branch may be stable within the framework of the present analysis. However, direct numerical simulations presented below demonstrate that, in the case $\Gamma_2 = 0$, the pinned soliton is always unstable against the displacement of its center from the point $x = 0$.

It may be relevant to compare these results with those that can be obtained for pinned solitons in the NLS model containing the loss and “hot spot”, see Eq. (15). NLS solitons may only exist if $D > 0$, therefore we adopt the normalization $D = 1$ in Eq. (15), and it makes sense to consider only the case when the inhomogeneity is attractive, i.e., $\Gamma_2 > 0$, otherwise the pinned soliton has no chance to be stable. Note that, once we choose $D > 0$ and $\Gamma_2 > 0$, the zero solution may be unstable, according to the results presented above.

In the conservative limit, $\gamma = \Gamma_1 = 0$, the pinned NLS soliton is given by a commonly known solution,

$$u = \eta \operatorname{sech}(\eta(|x| + a)) \exp\left(\frac{i}{2}\eta^2 t\right), \quad (34)$$

$$a = \frac{1}{2\eta} \ln\left(\frac{\eta + \Gamma_2}{\eta - \Gamma_2}\right), \quad (35)$$

where η is an intrinsic parameter of the solution family. Note that, as we assume $\Gamma_2 > 0$, Eq. (35) yields $a > 0$, hence the expression (34) has a single maximum at $x = 0$.

If now γ and Γ_2 are introduced as small parameters, the energy-balance condition for this solution can be easily cast in the form $\eta = -\Gamma_2 + 2\gamma/\Gamma_1$. In view of the relation (35), the actual solution exists in the region $\eta > \Gamma_2$, or, eventually, in the interval

$$0 < \Gamma_1 < \gamma/\Gamma_2. \quad (36)$$

Comparing this result with the expression (20) that determines the instability threshold for the zero solution, and taking into regard that $D = 1$, we conclude that the pinned soliton singled out by the balance condition disappears [crosses into the unphysical region, cf. Fig. 1(a)], with the increase of the stress parameter, Γ_1/γ , exactly at the point where the zero solution loses its stability. According to the above-mentioned stability exchange principle, this implies that the zero solution inherits its instability from the soliton, hence the soliton solution, given by Eqs. (34) and (35), is definitely *unstable* in all the region of its existence.

This conclusion demonstrates that the above results for the pinned solitons in the BG model are nontrivial, as they give the pinned gap soliton a chance to be stable, which is not possible at all in the simpler NLS model. Actual stability of the pinned gap solitons will be studied below by means of direct simulations.

III. NUMERICAL RESULTS FOR PINNED SOLITONS

A. The approximation for the delta-function

For the simulations, we have to adopt a numerical form of the δ -function in Eqs. (1),(2) and (5), (6). We use the same numerical scheme as in the recent work [14]. The scheme discretizes the coordinate x by 501 grid points x_j , $j = -250, \dots, -1, 0, +1, \dots + 250$. As an approximation to the δ -function, the following function is defined on a set of $2N + 1$ grid

points in the central part of the integration domain, located symmetrically around zero,

$$\tilde{\delta}(x_{n-(N+1)}) \equiv \begin{cases} A \cos\left(\frac{n-(N+1)\pi}{2N+1}\right) & \text{for } n = 1, \dots, 2N+1, \\ 0 & \text{elsewhere.} \end{cases} \quad (37)$$

The normalization factor A is defined so as to maintain the canonical normalization of the δ -function, $\int_{-\infty}^{+\infty} \tilde{\delta}(x) dx \equiv \sum_j \tilde{\delta}(x_j) \Delta x = 1$, which yields

$$A = \left[\Delta x \sum_{n=1}^{2N+1} \cos\left(\frac{n-(N+1)\pi}{2N+1}\right) \right]^{-1}, \quad (38)$$

Δx being the spacing of the grid (in fact, $\Delta x = 0.04$). In most cases presented below, we use $N = 2$ [then Eq. (38) with $\Delta x = 0.04$ yields $A = [(1 + \sqrt{5}) \Delta x]^{-1} \approx 7.726$], which makes the δ -function quite narrow indeed.

B. Stability of the pinned solitons in the conservative model

Since exact stationary solutions to Eqs. (5) and (6) for the pinned soliton are available in the case $\gamma = \Gamma_1 = 0$, in the form of Eq. (23) supplemented by Eq. (24), numerical test of their stability is straightforward. We simulated the stability by means of the split-step method applied to Eqs. (1) and (2), employing the fast Fourier transform. The exact solution (23) was taken as the initial configuration, and the corresponding value θ_{in} of θ was varied. The values $\theta_{\text{in}} < |\Gamma_2|$, at which the exact solution does not exist [see Eq. (26)] were probed too. In this case, Eq. (24) yields an imaginary value of a , and the initial configuration was taken in the form of Eq. (23) with the imaginary a . Even though the latter configuration is not a stationary solution, it is still nonsingular and localized, so it can be used to launch the PDE simulation.

As expected from what was mentioned above, in the case $\Gamma_2 < 0$ all the pinned states of the solitons are found to be unstable. Solitons are pushed away from the point $x = 0$, in accord with the expectation that the inhomogeneity is repulsive. It was also observed that, as $|\Gamma_2|$ increases, at $\Gamma_2 \leq -0.7$ a small soliton is left behind around the point $x = 0$ after the main pulse has separated from it; however, the residual soliton is also unstable and gradually decays into radiation.

For positive Γ_2 , typical results regarding the stability of the pinned solitons are displayed in Fig. 2. A conclusion is that there is a *single value* $\theta_{\text{stab}} \approx \pi/2$ of the soliton parameter

θ , such that if $\theta_{\text{in}} < \theta_{\text{stab}}$, the soliton decays into radiation, as is seen in Fig. 2(a). Solitons with $\theta_{\text{in}} > \theta_{\text{stab}}$ relax into a stable one with $\theta = \theta_{\text{stab}}$, see Fig. 2(b). Finally, a soliton with $\theta_{\text{in}} = \theta_{\text{stab}}$ directly gives rise to the stable soliton, see Fig. 2(c).

The examples shown in Fig. 2 pertain to $\Gamma_2 = 0.4$, and similar results were obtained for other values of Γ_2 . Available computational power imposes a limitation on accuracy with which θ_{stab} can be identified. However, it was found that, for $\Gamma_2 = 0.1$, the decrease of the soliton's amplitude, which is defined as $|u(x=0)|$, is less than 1% after the evolution time $T = 200\pi$, if θ_{in} is taken from the interval $(0.49\pi < \theta_{\text{in}} < 0.52\pi)$, hence, in any case, $\theta_{\text{stab}}(\Gamma_2 = 0.1)$ belongs to the same interval. For a much larger value of the perturbation parameter, $\Gamma_2 = 1.1$, the corresponding interval is $0.51\pi < \theta_{\text{in}} < 0.55\pi$, hence $\theta_{\text{stab}}(\Gamma_2 = 1.1)$ belongs to this region. Generally, θ_{stab} slightly increases with Γ_2 .

Figure 3 summarizes these results in the form of a plot in the $(\Gamma_2, \theta_{\text{in}})$ plane, which shows the regions where the initial soliton relaxes to the stable one or decays into radiation. In the region $\theta_{\text{in}} < |\Gamma_2|$, where the initial configurations are not true stationary solutions, this configuration decays into radiation immediately.

These results, obtained for the conservative model with the local inhomogeneity of the refractive index, are very similar to those reported in Ref. [14] for the stability of the solitons pinned by an attractive inhomogeneity in the form of a local suppression of the Bragg grating. A noticeable common feature of the results is the existence of the *single* (up to the numerical accuracy available) value $\theta_{\text{stab}} \approx \pi/2$ of the parameter θ which the established soliton may assume. In both conservative models (the ones considered here and in Ref. [14]), θ_{in} relaxes to θ_{stab} if $\theta_{\text{in}} > \theta_{\text{stab}}$, and the soliton decays into radiation if $\theta_{\text{in}} < \theta_{\text{stab}}$, i.e., the soliton with $\theta = \theta_{\text{stab}}$ may be called a *semi-attractor*. In fact, it strongly resembles *semi-stable* solitons, which are stable against small perturbations in the linear approximation, but may be unstable if terms quadratic in the perturbations are taken into regard. Semi-stable solitons were recently studied in another context, as the so-called embedded solitons, see Ref. [20] and references therein.

The fact that all the solitons with $\theta_{\text{in}} > \theta_{\text{stab}}$, where θ_{stab} is slightly larger than $\pi/2$, relax to the value $\theta = \theta_{\text{stab}}$, may be related to a known property of the ordinary solitons in the unperturbed BG model ($\gamma = \Gamma_1 = \Gamma_2 = 0$): they are unstable if $\theta > \theta_{\text{cr}}^{(0)} \approx 1.011 \cdot (\pi/2)$ [11]. Thus, at least in the case when Γ_2 is small, it is natural to expect that any pinned soliton with $\theta > \pi/2$ will relax, as a result of the instability, to a value close to $\theta_{\text{cr}}^{(0)}$. What is less

obvious, is the decay of the solitons with $\theta < \theta_{\text{stab}}$, and the fact that θ_{stab} so weakly depends on Γ_2 (see Fig. 3).

C. The pinned soliton in the lossy medium with the localized gain

In direct simulations of the full model, which includes the loss and local gain, the exact solution (23) of the conservative version was again used as the starting point. The evolution of the solution was simulated at a fixed value of the loss parameter γ . The local gain Γ_1 was varied in order to determine its value(s) at which the soliton settles down to a stable pinned soliton.

Figure 4 shows the evolution of the soliton's amplitude, defined as $|u(x=0)|$, vs. t , when the localized gain Γ_1 is varied. The other parameters are fixed, so that

$$\Gamma_2 = 0.5, \gamma = 0.0316, \theta_{\text{in}} = 0.5\pi. \quad (39)$$

For a small value of Γ_1 ($\Gamma_1 = 0.04208$ in Fig. 4), which is insufficient to balance the loss, the soliton decays. For a slightly larger $\Gamma_1 = 0.04209$, the soliton's amplitude grows, then it temporarily settles down (at the value 1.47 in Fig. 4), and, eventually, regular oscillations set in. A long simulation, up to $t = 600\pi$ (see Fig. 4) shows that the intrinsic vibrations of the soliton are completely stable. The waveforms $|u(x, t)|$ and $|v(x, t)|$, obtained at the end of the simulation for $\Gamma_1 = 0.04209$, are shown in Figure 5(a).

When the gain Γ_1 is further increased, the initial growth of the soliton's amplitude is sharper; however, it is found that it again temporarily settles down to a nearly constant value close to the same level of 1.47 as above, which is followed by the onset of persistent oscillations. When Γ_1 is still larger, the eventual oscillatory state becomes chaotic with large fluctuations. The corresponding waveforms of $|u(x)|$ and $|v(x)|$ at the end of the simulation ($t = 300\pi$) for $\Gamma_1 = 0.057$ are shown in Fig. 5(b). It can be seen that conspicuous radiation tails are attached to the soliton, which implies a permanent energy leakage from it. This extra loss adds up to the direct dissipative loss, both being compensated by the localized gain. If Γ_1 is too large, the radiation wave field outside the main pulse grows to such an extent that the resulting waveform cannot be regarded as a localized one. In fact, in this case it is observed that the main pulse separates from the point $x = 0$, drifts away, and dies down due to the loss. However, the strong localized gain generates a new "soliton" around

$x = 0$, which later drifts away again, this process repeating itself quasi-periodically.

An important feature of these results is that a stable (even though it is vibrating) soliton is possible not at a single value of the gain, that exactly compensates the loss, but in a finite interval of values of the gain. The energy balance is maintained, in this case, through permanent emission of radiation by the soliton, which compensates the excessive gain. It is relevant to mention that a very similar mechanism, which gives rise to stable *nonequilibrium solitons* in an overpumped system of a different type (that, however, also originates in nonlinear optics – the so-called split-step model), was recently considered in detail in Ref. [22]. In that case too, the stability of the soliton is provided by the emission of radiation that balances the excess gain.

A further insight in sustained intrinsic vibrations of the pinned soliton, and the transition from the regular oscillations to dynamical chaos, is provided by consideration of the spectrum of the function $|u(x = 0, t)|$. In the established oscillatory regime, the spectrum was computed at several different values of Γ_1 , while the other parameters were kept constant as per Eq. (39). Figure 6(a) shows the spectrum for $\Gamma_1 = 0.04209$, which is the value barely enough to compensate the loss. It can be seen that the established oscillations are quasi-harmonic, with a single well-pronounced frequency 2.9 (in arbitrary units), and an additional tiny spectral component at the frequency ≈ 2 (which is, apparently, incommensurate with the main one).

Figure 6(b) shows the spectrum for $\Gamma_1 = 0.5633$, which is similar to that in Fig. 6(a). The main frequency shifts down to a value about 2.8, with two other visible components found at the frequencies 0.8 and 1.4. Then, suddenly, at a slightly larger gain, $\Gamma_1 = 0.5634$, many new conspicuous spectral components emerge, which is shown in Fig. 6(c), and corresponds to (apparently) chaotic intrinsic vibrations of the established soliton. The same behavior is observed at $\Gamma_1 = 0.5635$. At $\Gamma_1 = 0.5636$, the picture suffers another abrupt change [see Fig. 6(d)]: the power spectrum reverts back to the simple three-frequency-component structure reminiscent of the situation at lower Γ_1 , cf. Fig. 6(b). A transition from a chaotic behavior, (presumably) accounted for by a strange attractor, to a simple quasi-harmonic behavior is known in the theory of dynamical systems, where it is called a “boundary crisis” of the chaotic attractor [21].

The picture revealed by the simulations changes the third time at $\Gamma_1 = 0.5640$, with reappearance of a many-component chaotic-like spectrum, similar to that in Fig. 6(c). The

chaotic behavior continues to higher values of Γ_1 . Figure 6(e) shows the spectrum at $\Gamma_1 = 0.05690$, where its structure is not simply a multi-component one, but continuous, which is characteristic for well-developed dynamical chaos.

Another way to describe basic properties of the pinned solitons in the full model is to identify, for various initial values of θ_{in} , a minimum value $(\Gamma_1)_{\text{min}}$ of the gain which is necessary to overcome the loss. Figure 7 shows the evolution of the soliton's amplitudes as a function of time for $\theta_{\text{in}} = 0.2\pi$, 0.5π , and 0.9π , the corresponding minimum values being $(\Gamma_1)_{\text{min}} = 0.0239$, 0.0133 , and 0.0131 , while the other parameters are fixed, $\gamma = 0.01$ and $\Gamma_2 = 0.5$ [note that all these values of θ_{in} exceed Γ_2 , hence the corresponding exact solitons in the conservative model do exist, according to Eq. (26)]. Thus, unlike the conservative model, in the full model, values of θ_{in} essentially smaller than $\pi/2$ may give rise to a stable pinned soliton (with intrinsic vibrations). However, the smaller the difference $\theta_{\text{in}} - \Gamma_2$, the larger value of Γ_1 is necessary, as, according to Eqs. (29) and (25), the rate at which the localized gain supplies energy to the soliton decreases $\sim (\theta_{\text{in}} - \Gamma_2)$ as $\theta_{\text{in}} - \Gamma_2 \rightarrow 0$. On the other hand, analysis of the simulation results shows that the characteristics of the established soliton do not depend on the initial value of θ_{in} which excited it, but solely on the values of γ and $\Gamma_{1,2}$, i.e., the established soliton is a genuine *attractor*.

Then, effects caused by varying the loss parameter γ were investigated. Because of the necessity to satisfy the energy balance condition, Γ_1 needs to be changed to track the variation of γ . For each value of γ , we tried to find the minimum size of Γ_1 that supports a stable soliton. Results of these numerical experiments, obtained for fixed $\Gamma_2 = 0.5$ and $\theta_{\text{in}} = \pi/2$, and a set of values $\gamma = 0.000316, 0.001, 0.00316, 0.01, 0.0316$, and 0.1 , are displayed in Fig. 8. The respective minimum-gain values were found to be $(\Gamma_1)_{\text{min}} = 0.000422, 0.00140, 0.00422, 0.0133, 0.04209$, and 0.1327 . It is interesting to note that, except for the second case, when the ratio $(\Gamma_1)_{\text{min}}/\gamma$ is 1.40 , in all the other ones the ratio takes values between 1.32 and 1.34 .

It is clearly seen from Fig. 8 that the amplitude of the established soliton monotonically increases with the growth of γ (which is accompanied by the growth of the minimum gain necessary to support the soliton). It is also seen that it was never possible to produce a truly stationary soliton, but in some cases ($\gamma = 0.000316, 0.00316, 0.01$, and 0.1) it was possible to generate nearly stationary solitons with a small amplitude of intrinsic vibrations. In other cases ($\gamma = 0.001$ and 0.0316), varying Γ_1 by steps as small as it was admitted by

the numerical scheme, it was *not* possible to adjust the gain so that to suppress the internal vibrations, i.e., the established soliton remained a breather, rather than anything close to a fixed-point state.

In all the cases presented in Fig. 8, γ and Γ_1 are small enough to treat them as perturbations. Then, if the established soliton assumes a nearly stationary form, it is natural to expect that it must be close to the solution (23) found in the conservative model, with some value of θ , and this θ must be related to γ and Γ_1 as per Eq. (31).

It was checked that the quasi-stationary solitons, in those cases in when they were found, are indeed close to the wave form (23). The corresponding values of θ were identified by means of the least-squared-error fit to the expression (23). Then, for thus found values of θ and given values of γ , the equilibrium values of the gain Γ_1 were calculated as predicted by the analytical formula (31). Results of this are presented in Table 1.

A noticeable fact obvious from Table 1 is that, in all the cases, the numerically found equilibrium value of the gain exceeds the analytically predicted one by 9 to 14 per cent. Because in all the cases, as it was stressed above, the established solitons are not completely stationary, a natural conjecture is that the slightly vibrating soliton continuously emits energy at a low rate, and this extra energy loss makes it necessary to have the gain somewhat larger than that which compensates the direct dissipative loss as per Eq. (31).

As concerns the comparison of the full model with its conservative counterpart, we recall that, in the conservative model, the stable pinned soliton always assumes a single value of θ for given Γ_2 (and this value very weakly depends on Γ_2 , always being slightly larger than $\pi/2$, see Fig. 3). On the contrary to this, in the full model the quasi-stationary soliton may be stable in a range of the values of θ , as it is evident from Table 1.

Finally, it has also been checked whether stable pinned solitons can be found when the “hot point” does not perturb the refractive index, i.e., $\Gamma_2 = 0$. As a result, it has been concluded that any finite positive Γ_2 (the smallest value tried was $\Gamma_2 = 0.01$) may support a stable soliton in the pinned state, but if $\Gamma_2 = 0$, the pulse set at $x = 0$ finally drifts away, and then decays due to the loss. An explanation to this finding may be that all the solitons found in the model with loss and gain emit some radiation, see above, and asymmetric fluctuations in the emission rate create a weak random force that drives the soliton away.

D. Soliton pinned between two repulsive inhomogeneities

The soliton may be stably pinned not only by an attractive inhomogeneity, but also between two separated repulsive ones (in the present context, each one will represent a locally suppressed refractive index, corresponding to $\Gamma_2 < 0$). The consideration of this configuration is interesting by itself, and it also may be used to design a soliton-based optical oscillator, in which the eigenfrequency is easily controlled by the choice of the separation between the two repulsive points. In particular, in the framework of the perturbation theory (for small $|\Gamma_2|$), the soliton may be regarded as a quasiparticle in the external potential

$$W_2(\xi) = W_1\left(\frac{1}{2}L - \xi\right) + W_1\left(\frac{1}{2}L + \xi\right), \quad (40)$$

where the potential $W_1(\xi)$ is given by Eq. (27) (with $\Gamma_2 < 0$), and L is the separation between the two defects.

We simulated the dynamics of this configuration in some detail, but only for the conservative case, $\gamma = \Gamma_1 = 0$. First of all, if L is smaller than the proper size of the soliton, it sees the pair of the inhomogeneities, in the first approximation, as a single repulsive center, hence stable bound states are not possible. Within the framework of the perturbation theory, Eqs. (40) and (27) make it possible to predict a critical value, $(\Delta\xi)_{\text{cr}}$, at which a stable equilibrium appears for the first time at $x = 0$. The corresponding expression is cumbersome, but it is easy to verify that $(\Delta\xi)_{\text{cr}}$ monotonically decreases, with θ varying from 0 to $\pi/2$, from $(\Delta\xi)_{\text{cr}} = \infty$ to the minimum value $(\Delta\xi)_{\text{cr}} = \ln(\sqrt{2} + 1) \approx 0.88$.

Direct simulations at finite Γ_2 demonstrate [see an example in Fig. 9] that, in the case of relatively small L , when the pinned state of the soliton is unstable, the dynamical evolution does not trivially reduce to pushing the soliton aside; instead, a generic outcome is *splitting* of the soliton in two, which is accompanied by a spontaneous symmetry breaking (in some cases, for instance if $\theta_{\text{in}} = 0.7\pi$, the other parameters being the same as in Fig. 9, the instability develops so slowly that it was not possible to identify the outcome).

With the increase of L , stabilization of the soliton trapped between the repulsive inhomogeneities becomes possible. The trapped states seem most stable around the value $L = 3.84$, see an example in Fig. 10. In this case, systematic simulations reveal a feature which strongly resembles the one reported above for the single attractive inhomogeneity in the conservative model: an established trapped state is stable for a single (up to the accuracy

of numerical simulations) value of θ , which is very close to $\pi/2$; if $\theta_{\text{in}} > \pi/2$, the soliton sheds off some radiation and eventually relaxes to the said single value of θ (see Fig. 10), while if $\theta_{\text{in}} < \pi/2$, the soliton gradually decays into radiation. Thus, the single-valuedness of the stable soliton in the conservative model appears to be a generic property. For still larger values of L , the pinned state is less robust; in particular, a soliton with $\theta_{\text{in}} > \pi/2$ may split, instead of relaxing to the stable one with $\theta \approx \pi/2$.

IV. COLLISION OF A MOVING SOLITON WITH THE LOCALIZED GAIN

Once the existence of stable pinned soliton has been established, the next natural step is to consider a possibility of capturing a free moving soliton by the “hot spot”. To this end, the soliton was first generated far from the spot by means of the Newton-Raphson method, as a stationary solution in the reference frame moving at some velocity c ; a range of the velocities $0 \leq c \leq 0.7$ was thus investigated. Then, the collision was considered, running direct simulations of Eqs. (1) and (2).

First, the collision experiment was performed in the conservative model, with $\Gamma_1 = \gamma = 0$. The parameter plane (c, Γ_2) was explored with c taking values 0.1, 0.2, \dots , 0.7, and Γ_2 taking values 0.1, 0.2, \dots , 0.9, while θ_{in} was kept constant at 0.7π .

If the inhomogeneity is weak, the moving soliton passes through it, see an example in Fig. 11(a). When the inhomogeneity strength is larger, $\Gamma_2 \gtrsim 0.5$, a part of the soliton still passes through it, but another part of the soliton’s energy is captured by the local defect to form a pinned soliton, an example of which is shown in Fig. 11(b). Some radiation bouncing in the backward direction can also be observed when Γ_2 is large, or when the incident soliton is fast. Naturally, more energy is trapped by the defect if Γ_2 is larger [Fig. 11(c)], and less energy is trapped if the soliton is faster. However, the value $\Gamma_2 \approx 0.5$, at which the trapping begins, only weakly depends on the soliton’s velocity c . Figure 12 summarizes these results, showing a border in the (c, Γ_2) plane between the passage and partial-capture regions.

Next, we consider the collisions in the full model, with $\gamma = 0.01$ and $\Gamma_1 = 0.015$. Results reported in the previous section show that a stable pinned soliton exists at these values of the loss and gain (the collisions were simulated only for small values of γ , as otherwise the soliton will be strongly attenuated still before the collision). The initial value of the soliton’s parameter was again $\theta_{\text{in}} = 0.7\pi$.

The results obtained for the full model are not very different from those for the conservative one. When the gain Γ_2 is small, the soliton passes through, and if Γ_2 is larger, a part of the energy is trapped to form a pinned soliton. A difference from the conservative model is that the value of Γ_2 at which the inhomogeneity starts to capture a part of the soliton's energy in the conservative model is approximately independent of its velocity: $\Gamma_2 \approx 0.5$ if $c > 0.1$, while in the lossy model, this value of Γ_2 increases with c , as is seen in Fig. 12.

Another representative set of numerical data can be displayed for a fixed value of the soliton's velocity, $c = 0.1$, while the parameter θ_{in} of the incident soliton takes values $0.1\pi, 0.2\pi, \dots, 0.9\pi$, and $\Gamma_2 = 0.1, 0.2, \dots, 0.9$. These results are presented here only for the conservative model.

Simulations show that, if the moving soliton is heavy (large θ_{in}) or the inhomogeneity is weak, the soliton passes it. Heavier solitons can pass through a stronger defect. If the inhomogeneity is strong (Γ_2 is large), the soliton gets trapped, which is always accompanied by emission of radiation in both the forward and backward directions, and the radiation can further self-trap into secondary solitons. At small Γ_2 , little energy is scattered away in either direction. If Γ_2 is larger, more energy is scattered forward, and when Γ_2 is still larger ($\Gamma_2 \approx 0.9$), more energy is scattered backwards, cf. Fig. 11(c). Figure 13 summarizes the results obtained for the interaction of the moving soliton and the localized attractive defect in the conservative model for the fixed velocity, $c = 0.1$

It is natural to compare the results obtained for the conservative model with those reported in Ref. [14] for the interaction of the moving gap soliton with an attractive inhomogeneity in the form of a local suppression of the Bragg grating. In that case, when the soliton was heavy (large θ), the interaction effectively reverted from attraction to repulsion, so that the incident soliton could bounce back. In the present model, this unusual behavior has never been observed.

V. CONCLUSION

In this work, we have introduced a model of a lossy nonlinear fiber grating with a “hot spot” combining the localized gain and attractive inhomogeneity of the refractive index; the spot can be created by means of doping a short segment of the fiber. In the absence of the loss and gain, a family of exact solutions for pinned solitons was found. In the full model

including loss and gain, the instability threshold for the zero solution was found; it was concluded that the instability is not possible without the presence of the imaginary part of the local gain, i.e., a localized perturbation of the refractive index. Further, for small values of the loss and gain, it was predicted what soliton is selected by the energy-balance condition. Parallel to this, it was shown that, in the simpler model based on the NLS equation, the pinned soliton can never be stable in the presence of the loss and local gain.

In direct simulations, we have found that a single pinned soliton is stable in the conservative fiber-grating model. It is a semi-attractor: solitons with a larger energy relax to it via emission of radiation, while the ones with smaller energy completely decay into radiation. The same conclusion is obtained for solitons trapped between two repulsive inhomogeneities. In the full model with the loss and gain, all the stable pinned pulses demonstrate persistent internal vibrations and emission of radiation. Sometimes, they are almost stationary solitons, and in these cases the prediction based on the energy balance underestimates the necessary gain by 9% to 14%, which is explained by the extra radiation loss. If the loss and gain increase, the intrinsic vibrations become chaotic.

Collisions of free moving solitons with the “hot spot” were simulated too. The passage and capture regimes were identified for the solitons in the conservative and full models; the capture is only partial, which actually implies splitting of the soliton. It was also found that, if a large part of the soliton’s energy is radiated away, it may self-trap into secondary solitons.

Acknowledgement

B.A.M. appreciates hospitality of the Optoelectronic Research Centre at the City University of Hong Kong.

-
- [1] G.P. Agrawal. *Nonlinear Fiber Optics* (Academic Press: Boston, 1995).
- [2] R. Kashyap. *Fiber Bragg gratings* (Academic Press: San Diego, 1999).
- [3] J. Marangos, “Slow light in cool atoms”, *Nature* **397**, 559-560 (1999); K.T. McDonald, “Slow light”, *Am. J. Phys.* **68**, 293-294 (2000).
- [4] C.M. de Sterke and J.E. Sipe, “Gap solitons”, *Progr. Opt.* **33**, 203-260 (1994).
- [5] A.B. Aceves and S. Wabnitz, “Self-induced transparency solitons in nonlinear refractive periodic media”, *Phys. Lett. A* **141**, 37-42 (1989).
- [6] D.N. Christodoulides and R.I. Joseph, “Slow Bragg solitons in nonlinear periodic structures”, *Phys. Rev. Lett.* **62**, 1746-1749 (1989).
- [7] B.J. Eggleton, R.E. Slusher, C.M. de Sterke, P.A. Krug, and J.E. Sipe, *Phys. Rev. Lett.* **76**, 1627 (1996); C.M. de Sterke, B.J. Eggleton, and P.A. Krug, *J. Lightwave Technol.* **15**, 1494 (1997).
- [8] N.M. Litchinitser, B.J. Eggleton, C.M. de Sterke, A.B. Aceves, and G.P. Agrawal, “Interaction of Bragg solitons in fiber gratings”, *J. Opt. Soc. Am. B* **16**, 18-23 (1999).
- [9] J.E. Heebner, R.W. Boyd, and Q.H. Park, “Slow light, induced dispersion, enhanced nonlinearity, and optical solitons in a resonator-array waveguide”, *Phys. Rev. E* **65**, 036619 (2002).
- [10] B.A. Malomed and R.S. Tasgal, “Vibration modes of a gap soliton in a nonlinear optical medium”, *Phys. Rev. E* **49**, 5787-5796 (1994).
- [11] I.V. Barashenkov, D.E. Pelinovsky, and E.V. Zemlyanaya, “Vibrations and Oscillatory Instabilities of Gap Solitons”, *Phys. Rev. Lett.* **80**, 5117-5120 (1998).
- [12] C.M. de Sterke, E.N. Tsoy, and J.E. Sipe, “Light trapping in a fiber grating defect by four-wave mixing”, *Opt. Lett.* **27**, 485-487 (2002).
- [13] R.H. Goodman, R.E. Slusher, and M.I. Weinstein, “Stopping light on a defect”, *J. Opt. Soc. Am. B* **19**, 1635-1652 (2002).
- [14] W.C.K. Mak, B.A. Malomed, P.L. Chu, “Interaction of a soliton with a local defect in a fiber Bragg grating”, submitted to *J. Opt. Soc. Am. B*.
- [15] B.J. Eggleton, T. Stephens, P.A. Krug, G. Dhozi, Z. Brodzeli, and F. Ouellete, *Electr. Lett.* **32**, 1610 (1996).
- [16] S.I. Najafi, T. Touam, R. Sara, M.P. Andrews, and M.A. Fardad, *J. Lightwave Technol.* **16**,

1640 (1998).

- [17] E. Desurvire, *Erbium-Doped Fiber Amplifiers* (Wiley-Interscience: New York, 1994).
- [18] L. Gilles and P. Tran, “Optical switching in nonlinear chiral distributed Bragg reflectors with defect layers”, *J. Opt. Soc. Am. B* **19**, 630-639 (2002).
- [19] G. Iooss and D.D. Joseph. *Elementary Stability and Bifurcation Theory* (Springer-Verlag: New York, Heidelberg, Berlin, 1980).
- [20] A.R. Champneys, B.A. Malomed, J. Yang, and D.J. Kaup, “Embedded solitons”: solitary waves in resonance with the linear spectrum”, *Physica D* **152-153**, 340-354 (2001).
- [21] R.C. Hilborn. *Chaos and Nonlinear Dynamics* (Oxford University Press: New York and Oxford, 1994).
- [22] R. Driben and B.A. Malomed, Equilibrium and nonequilibrium solitons in a lossy split-step system with lumped amplification, *Phys. Lett. A* **301**, 1926-1931 (2002).
- [23] Y.S. Kivshar and B.A. Malomed, “Dynamics of solitons in nearly integrable systems”, *Rev. Mod. Phys.* **61**, 763-915 (1989).
- [24] M.G. Vakhitov and A.A. Kolokolov, *Sov. J. Radiophys. Quantum Electr.* **16**, 783 (1973).

Tables

γ	θ	$(\Gamma_1)_{\text{num}}$	$(\Gamma_1)_{\text{anal}}$	$\frac{(\Gamma_1)_{\text{num}} - (\Gamma_1)_{\text{anal}}}{(\Gamma_1)_{\text{anal}}}$
0.000316	0.5π	0.000422	0.000386	0.0944
0.00316	0.595π	0.0042	0.00369	0.1373
0.01	0.608π	0.01333	0.01165	0.1442
0.1	0.826π	0.1327	0.121	0.0967

Table 1. Values of the loss parameter γ at which quasi-stationary stable pinned solitons were found by the adjustment of the gain Γ_1 (see Fig. 8), while the refractive-index perturbation is fixed, $\Gamma_2 = 0.5$. The corresponding values of the gain, $(\Gamma_1)_{\text{num}}$, are also included, together with the values of the soliton parameter θ which provide for the best fit of the quasi-stationary solitons to the analytical solution (23). The values $(\Gamma_1)_{\text{anal}}$ are those predicted, for given γ and θ , by the energy-balance equation (31), which does not take the radiation loss into account.

Figure captions

Fig. 1. Analytically predicted solution branches for the pinned soliton in the case of weak loss and gain. Shown is $\theta - \Gamma_2$ vs. the stress parameter Γ_1/γ . (a) An example of the case $\Gamma_2 < \pi/2$ is displayed with $\Gamma_2 = \pi/4$; (b) an example of the case $\Gamma_2 > \pi/2$ is displayed with $\Gamma_2 = 3\pi/4$; (c) $\Gamma_2 = \pi/2$; (d) $\Gamma_2 = 0$. In the last case, nontrivial solutions appear at the point $\theta = 0.7442\pi$, $\Gamma_1/\gamma = 1.3801$, and at large values of Γ_1/γ the continuous curve asymptotically approaches the horizontal axis. In all the panels, the dashed lines show a formal continuation of the solutions in the unphysical regions, $\theta < \Gamma_2$, and $\theta > \pi$. In the panels (a), (b), and (c), the trivial solution, $\theta - \Gamma_2 = 0$, is shown by the solid line where it is stable; in the case corresponding to the panel (d), all the axis $\theta = 0$ corresponds to the stable trivial solution. (Note that all quantities plotted are dimensionless.)

Fig. 2. Typical results illustrating the stability and instability of pinned solitons in the case $\gamma = \Gamma_1 = 0$, and $\Gamma_2 = 0.4$. Each panel shows the evolution of $|u(x, t)|$, starting with the exact pinned-soliton configuration (the evolution of $|v(x, t)|$ is quite similar.) (a) $\theta_{\text{in}} = 0.4\pi$ is smaller than θ_{stab} : the soliton decays into radiation. (b) $\theta_{\text{in}} = 0.8\pi > \theta_{\text{stab}}$: the initial soliton transforms itself into a stable one, shedding off excess energy in the form of radiation. (c) $\theta_{\text{in}} = 0.5\pi \approx \theta_{\text{stab}}$. Direct appearance of the stable soliton.

Fig. 3. A summary of results obtained for the stability of pinned solitons, plotted in the $(\Gamma_2, \theta_{\text{in}})$ plane, in the conservative model with $\gamma = \Gamma_1 = 0$. In the upper region, where $\theta > \theta_{\text{stab}}$, initial solitons evolve into the stable one, shedding off extra energy. In the lower region, where $\theta < \theta_{\text{stab}}$, solitons completely decay into radiation. Beneath the lower solid line, which borders the region where $|\Gamma_2| < \theta < \pi$, see Eq. (26), stationary solutions for the pinned solitons do not exist. Accordingly, an initial pulse taken as a formal “soliton”, with an imaginary root of Eq. (24) substituted for a (see the text), is immediately destroyed.

Fig. 4. Evolution of the amplitude of the pinned soliton in the full model with loss and gain, in the case with $\Gamma_2 = 0.5$, $\gamma = 0.0316$ and $\theta_{\text{in}} = 0.5\pi$. If $\Gamma_1 = 0.04208$, the gain is insufficient to balance the loss, and the soliton decays. When $\Gamma_1 = 0.04209$, the soliton initially grows, and its intrinsic vibrations develop. When Γ_1 takes a slightly larger value, 0.04215, the initial growth of the amplitude is steeper, which again results in the establishment of regular intrinsic vibrations (in this case, the oscillations are very similar to those supported by $\Gamma_1 = 0.04209$). When Γ_1 is essentially larger, for instance, $\Gamma_1 = 0.057$,

interal vibrations of the pinned soliton become chaotic (the latter case shown by the dotted line).

Fig. 5. The profiles of $|u(x, t)|$ (solid lines) and $|v(x, t)|$ (dashed lines) at the end of the simulation (narrow peaks placed at $x = 0$ mark the “hot spot”). The values of γ , Γ_2 , and θ_{in} are the same as in Fig. 4. (a) $\Gamma_1 = 0.04209$ is barely enough to support the soliton against the loss. In this case, the soliton emits radiation at a low rate. (b) $\Gamma_1 = 0.057$. The soliton emits radiation at a high rate.

Fig. 6. The frequency spectrum of the time-dependent amplitude $|u(x = 0, t)|$ of the pinned soliton at different values of the local gain Γ_1 , after persistent vibrations set it: (a) $\Gamma_1 = 0.04209$, (b) $\Gamma_1 = 0.05633$, (c) $\Gamma_1 = 0.05634$, (d) $\Gamma_1 = 0.5636$, and (e) $\Gamma_1 = 0.05690$. In all the cases, $\gamma = 0.0316$, $\Gamma_2 = 0.5$, and $\theta_{\text{in}} = 0.5\pi$.

Fig. 7. The soliton’s amplitude $|u(x = 0, t)|$ vs. t for three different values of the initial amplitude θ_{in} . In each case, the value of the gain Γ_1 is chosen as the minimum one which can support the establishment of a soliton. Other parameters are fixed: $\Gamma_2 = 0.5$, and $\gamma = 0.01$.

Fig. 8. The amplitude of the soliton, $|u(x = 0, t)|$, vs. t for different values of the loss parameter γ . Each time, the value of the gain Γ_1 is chosen as the smallest one which leads to the establishment of the soliton. Other parameters are fixed: $\Gamma_2 = 0.5$, and $\theta_{\text{in}} = 0.5\pi$.

Fig. 9. The interaction of a soliton with a pair of repulsive points ($\Gamma_2 = -0.7$), with a relatively small separation between them, $L = 1.84$, in the conservative model. (a) The initial configuration, with $\theta_{\text{in}} = \pi/2$. (b) The result of the interaction: splitting of the soliton into two pulses, which is accompanied by a spontaneous symmetry breaking. The solid lines show $|u|$, and the dashed lines show $|v|$. Note that, in the initial configuration, $|u|$ and $|v|$ are indiscernible.

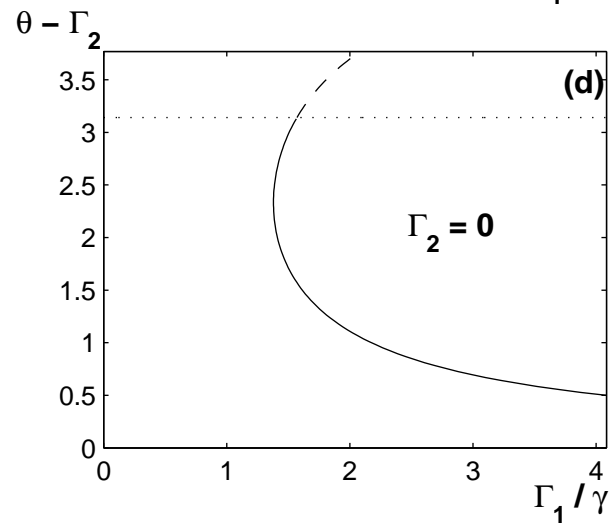
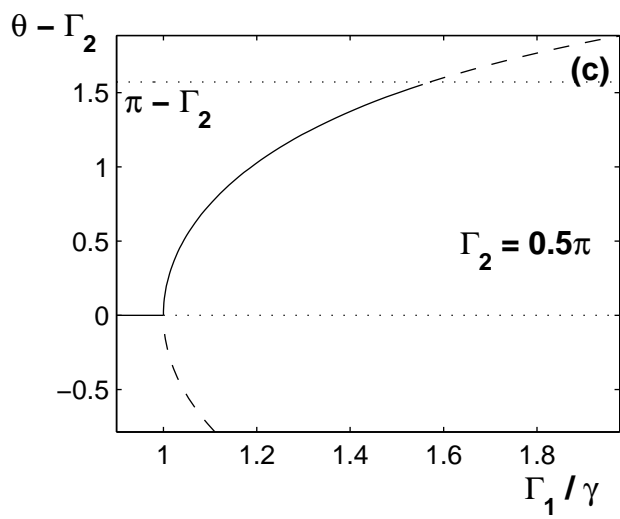
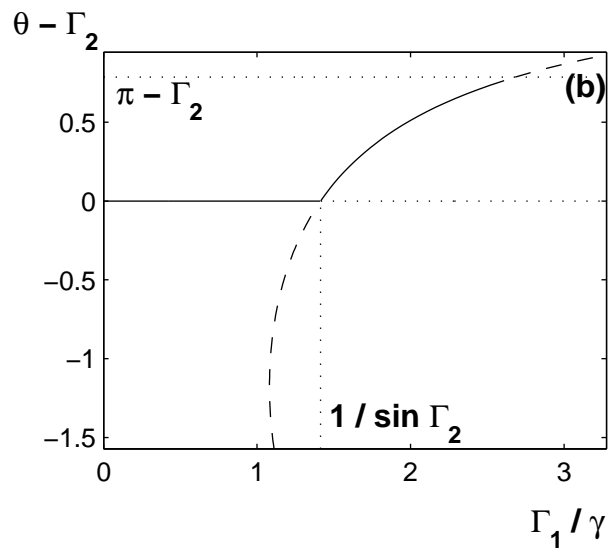
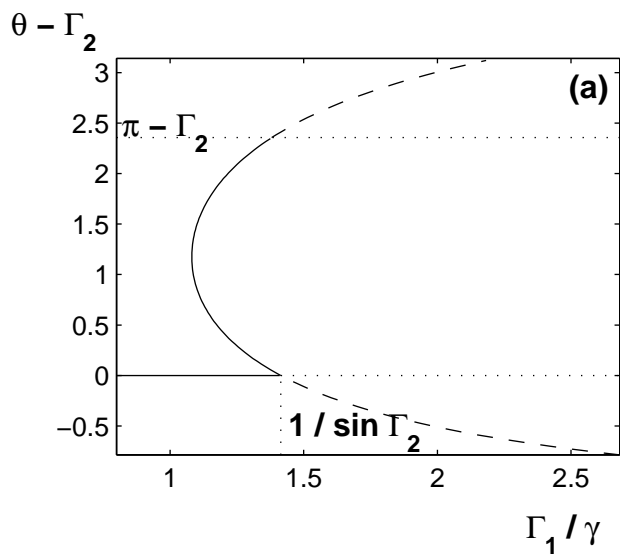
Fig. 10. Stable soliton captured between the repulsive points ($\Gamma_2 = -0.5$) with the separation $L = 3.84$ between them, in the conservative model. Shown is the evolution of the field $|u(x, t)|$. The initial value of the soliton parameter is $\theta_{\text{in}} = 0.7\pi$.

Fig. 11. Collision of a moving soliton, with fixed values $\theta = 0.7\pi$ and $c = 0.4$, and the inhomogeneity in the conservative model (the inhomogeneity is shown by a narrow peak which, for an unessential reason, is shifted from the point $x = 0$). The lower and upper panels show, respectively, the evolution of the field $|u(x, t)|$ in terms of the contour plots, and the waveforms $|u(x)|$ and $|v(x)|$ (solid and dashed lines) at the end of the simulation

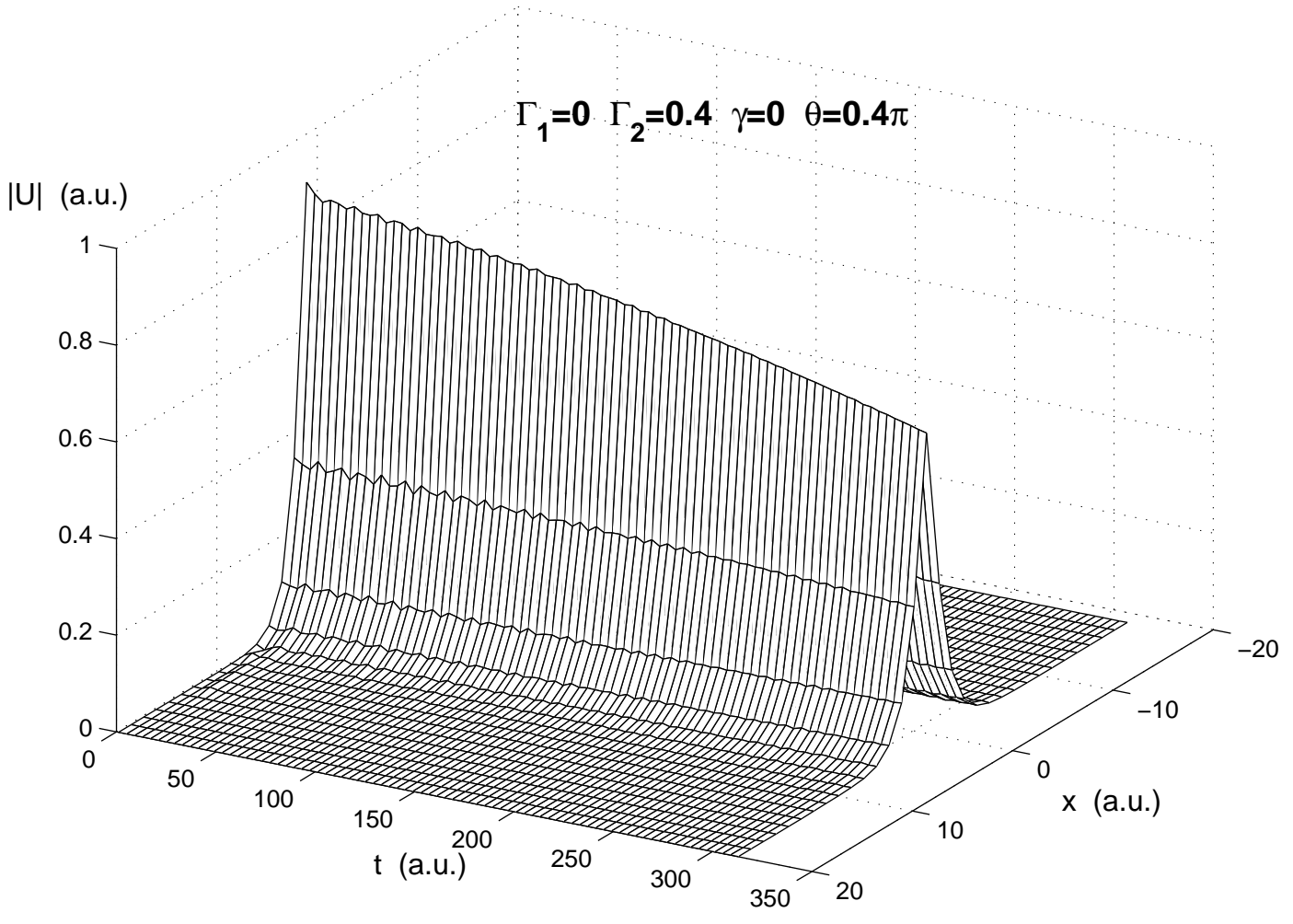
(note that the u - and v -components are asymmetric in the moving solitons). (a) The soliton passes through a weak defect with $\Gamma_2 = 0.2$. (b) A stronger defect, with $\Gamma_2 = 0.5$, captures a part of the energy of the passing soliton, to form a small-amplitude pinned one. Another small part of the energy bounces back in the form of radiation. (c) If the defect is still stronger, $\Gamma_2 = 0.9$, the shares of the trapped and bounced energy are larger.

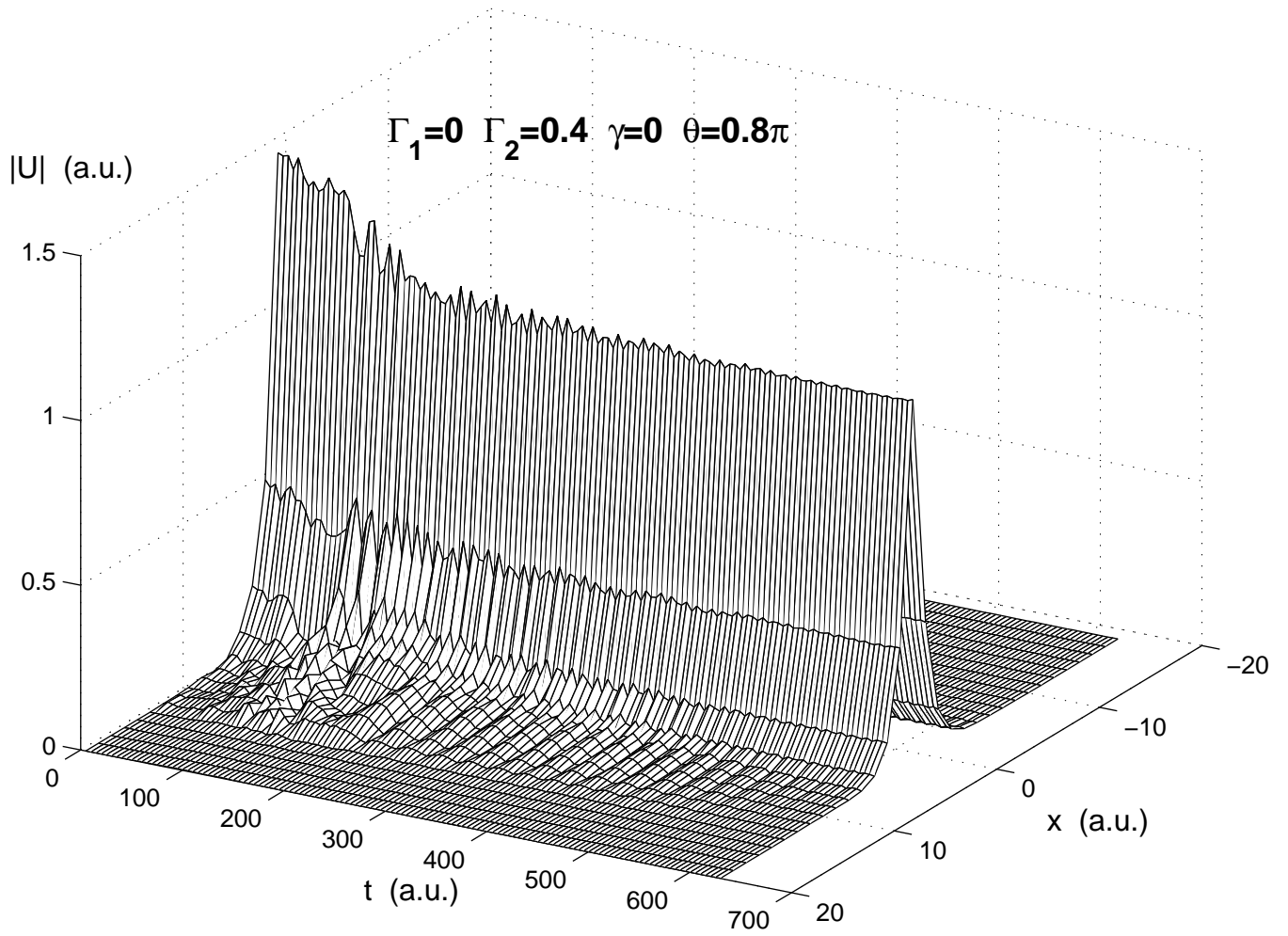
Fig. 12. Borders in the parametric plane (c, Γ_2) between regions in which the moving soliton with fixed $\theta = 0.7\pi$ passes the defect or gets partially trapped. The solid line is the border in the conservative model, with $\gamma = \Gamma_1 = 0$. The dashed line is the border in the full model with $\gamma = 0.01$ and $\Gamma_1 = 0.015$.

Fig. 13. Regions in the parametric plane (θ, Γ_2) of the conservative model in which the moving soliton with fixed $c = 0.1$ passes the defect or gets partially trapped.



$\Gamma_1=0 \quad \Gamma_2=0.4 \quad \gamma=0 \quad \theta=0.4\pi$





$\Gamma_1=0 \quad \Gamma_2=0.4 \quad \gamma=0 \quad \theta=0.5\pi$

